Desalination and Water Treatment
www.deswater.com

doi:10.5004/dwt.2019.24598

166 (2019) 144–157
October

S-N codoping TiO_2/SiO_2 and $TiO_2/SiO_2/Fe_3O_4$ core-shell nanocomposites as a novel purple LED light driven photocatalyst for degradation of paracetamol: optimization and different scavenger agents study

Zahra Amini, Mohammad Hadi Givianrad*, Seyd Waqif Husain, Parviz Aberoomand Azar, Mohammad Saber-Tehrani

Department of Chemistry, Science and Research Branch, Islamic Azad University, Tehran, Iran,
email: amini.zahra67@yahoo.com (Z. Amini), Tel. +982144868449, Fax +982144868445,
email: givianradh@yahoo.com (M.H. Givianrad), syedwaqifhusain@yahoo.com (S. Waqif Husain),
parvizaberoomand@gmail.com (P. Aberoomand Azar), drmsabertehrani@yahoo.com (M. Saber-Tehrani)

Received 15 December 2018; Accepted 20 June 2019

ABSTRACT

S-N codoping TiO_2/SiO_2 as a novel purple LED light active photo catalyst have been prepared by simple sol-gel method. The Fe_3O_4 magnetic particles were also used as the core to create recoverable photo catalysts. The results indicated that the photo catalytic activity of TiO_2 increases with the addition of thiourea as a source of nitrogen and sulfur in the visible light range. Moreover, the SiO_2 coupling increased the titanium dioxide active surface, reinforcing its photo catalytic properties. The prepared samples were characterized by XRD, BET, BJH, DRS-UV/Vis, PL, FESEM, EDX, TEM, VSM and XPS analysis. The XRD results revealed that the undoped and codoped TiO_2 nanoparticles only had the anatase phase. The photo catalytic effect of the synthesized nanoparticles on paracetamol degradation was also studied. The central composite design was employed to optimize the operational parameters including irradiation time, pH, photo catalyst mass and paracetamol concentration. The optimum values obtained were 164.53 min, 4.53, 00.11 g, and 15.24 mg L^{-1} for irradiation time, pH, photo catalyst mass and paracetamol concentration, respectively. Under the optimum conditions, the photo catalytic degradation percentages of paracetamol at desirability function value of 1.0 were found to be 99.98%. GC /MS was used to determine the photo catalytic degradation products of paracetamol. The photo catalytic activity of the nanoparticles was also studied under sunlight. Consequently, the UV/Vis spectrophotometry and TOC results showed that the synthesized nanoparticles have an extraordinary photo catalytic activity for the destruction of paracetamol under both purple LED and solar lights. Furthermore, different scavenger agents were investigated.

Keywords: Paracetamol; Codoped TiO_2; Photo catalyst; LED light; Scavenger agents

1. Introduction

Recently, besides the protection of water resources and proper use of water, some of the most important issues have been water and wastewater treatment. Regarding wastewater treatment, the presence of carcinogenic organic compounds is a major issue [1,2]. Pharmaceutical compounds comprise an important group of organic pollutants by virtue of their toxicity. These compounds have been recently spotted in liquid effluents, surface and groundwater resources, and even drinking water resources [3–6]. Some of the destructive effects of pharmaceutical pollutants on health are aquatic toxicity, resistance to pathogenic bacteria, genetic toxicity, and endocrine disorders [7–9]. The low concentration of pharmaceutical compounds and other exocentric compounds in drinking water has heightened public concerns. This is because there is little information on the possible chronic health-related effects of the long-term digestion of these compounds in drinking water [10].

*Corresponding author.

These compounds find their way into water resources through various means such as the direct disposal of unwanted drugs at homes, human and animal excretions, and ineffective processing of industrial sewage [5,11]. Acetaminophen (acetamide N-4-hydroxyphenylpyru) is a common analgesic and antipyretic drug commonly known as paracetamol (PA). This drug is one of the three most prescribed drugs with an annual global intake of 100 tons [12]. Accordingly, there is a need for an effective system capable of removing organic pollutants from aquatic environments.

The conventional water and wastewater treatment processes fail to decompose and remove these compounds. In addition, various methods such as activated carbon adsorption, reverse osmosis and biological techniques have been used to remove these organic pollutants. However, these methods do not eliminate the pollutants as they only fuel its transition from one phase to another [13–15]. Among the other methods, advanced oxidation processes (AOP) are more commonly used to treat waste waters. This is because these methods do not solely transfer pollution from one phase to another. Instead, they convert the pollutants into safer compounds such as H_2O and CO_2 unlike the other methods [16,17].

Semiconductor photo catalysts are also among the most reliable advanced oxidation processes designed to eliminate water soluble pollutants. As one of the existing semiconductor photo catalysts, TiO_2 is the most reliable solution for removing organic pollutants owing to its efficiency, nontoxicity, durability, low cost, high oxidation potential, and ease of storage [18–21]. However, the wide band gap of TiO_2 (3.2 eV for the anatase phase) and the high rate of electron-hole recombination are the pitfalls of the extensive usage of this valuable substance in the visible spectrum [18,22].

Various methods of overcoming these weaknesses and limitations of TiO_2 have been analyzed [18]. One of these effective methods involves the doping and codoping of metals and nonmetals, which can reduce the band gap energy in TiO_2 by creating defects in the TiO_2 crystalline structure [23]. The previous research results also suggested that the doping of nonmetals such as F, S, C, B and N with TiO_2 diminishes the recombination properties and improves the photo catalytic activity of these nanoparticles under the visible lights with a wavelength of more than 400 nm [24,25]. The codoping of TiO_2 with nonmetals such as B and N [26,27], Ni and Pt [28,29], N and F [30], S and N [31–34], has also garnered considerable attention because of the improved photo catalytic properties of TiO_2. Khalilian et al. synthesized a sulfur and nitrogen codoped TiO_2 for photo catalytic destruction of methyl orange under visible irradiation [31]. Yao et al. prepared S-N codoped TiO_2 at low temperature condition activated under visible irradiation [32].

Moreover, another effective method of reinforcing the photo catalytic effect increases the active site on the TiO_2 surface by combining it with other semiconductors [35]. SiO_2 is one of the most effective agents that increases the specific surface area, reduces the band gap, and prevents the photo catalyst transition from the anatase to rutile phase when combined with TiO_2 [36]. Anderson et al. examined mixing of SiO_2 into TiO_2 lattice and reported enhanced activity in degradation of rhodamine-6G than undoped TiO_2 [37]. Islam et al. utilized a crack-free sol-gel based TiO_2/SiO_2 hybrid nanoparticle films that resulted to homogeneous and less aggregated surface [38]. Wang et al. prepared mesoporous TiO_2/SiO_2 nanocomposites for photo catalytic degradation of arsenic [39].

One of the substantial problems following photo degradation is the removal of the photo catalyst, because it is in the nano-powder form. The separation and removal of the photo catalyst are time-consuming and expensive. The catalyst also deposits very slowly or it has to be centrifuged to be removed from the solution. An effective solution for overcoming these limitations is the use of magnetic particles that form the core of the magnetically recoverable photo catalyst. Very few studies have been conducted in the synthesis of core-shell $TiO_2/SiO_2/Fe_3O_4$ nanoparticles and their photo catalytic activity. Álvarez et al. reported magnetically separable $TiO_2/SiO_2/Fe_3O_4$ photo catalyst for photo catalytic degradation of emerging pollutant in water [40]. Gad-Allah et al. synthesized $TiO_2/SiO_2/Fe_3O_4$ nanocomposites in the form of patches and examined their photo catalytic activity [41].

In the present study, novel sulfur and nitrogen codoped TiO_2/SiO_2 (SNTS) and $TiO_2/SiO_2/Fe_3O_4$ (SNTSF) photo catalysts were synthesized by sol-gel method and then characterized. These nanophoto catalysts were used for degradation of PA under purple LED light and sunlight, which had not been carried out previously to our knowledge. The central composite design (CCD) method was used to optimize the operational parameters. The analysis results revealed the extraordinary capacity of the synthesized nanoparticles for removing PA from aquatic solutions under purple LED and solar light. Different scavenger agents and their effects on the degradation process were also studied.

2. Experimental

2.1. Preparation of S/N codoping TiO_2/SiO_2 and $TiO_2/SiO_2/Fe_3O_4$ nanocomposites

All the chemicals were purchased from Merck and used with no extra purification. The nanoparticles were synthesized by the sol-gel method. Tetrabutyl orthotitanate (TBOT) was used as the precursor for titania. Besides, 5 mL of TBOT, 20 mL of absolute ethanol, and 5 mL of acetyl acetone were mixed and blended for 30 min using a magnetic mixer to prepare the sol solution. Afterward, 4 mL deionized water was added to the mix and agitated continuously for a further 10 min. Then, the pH was adjusted at about 1.8 with concentrated HCl. Thiourea (CH_4N_2S) was utilized as the source of Nitrogen and Sulfur to improve the photo catalytic activity of TiO_2 under visible lights with a wavelength over 400 nm. To obtain the optimal and effective concentration of thiourea, all of the previous studies were reviewed and the optimal mole ratio of TU/TiO_2 was set to 0.4 based on the previous research [42]. After adding thiourea, the solution was mixed for 2 h. Next, the solution received 2 g of highly pure silica gel 60 (70–230 mesh) and mixed for an additional 2 h. The resulting sol solution was exposed to air for 24 h in a dark place in order to obtain the gel. Afterwards, the resulting gel was dehydrated in an oven for 4 h at 80°C. Calcination of the dehydrated sample was carried out in a furnace for 2 h at 500°C. The powdered nanoparticles (SNTS) all formed in the anatase phase.

The magnetic Fe_3O_4 nanoparticles were purchased from Sigma-Aldrich Company to produce the recoverable photo catalyst (using a magnetic field). The same steps were taken to synthesize the SNTSF except that after adding SiO_2, a certain amount of Fe_3O_4 was added to the solution, which was mixed for two hours. The weight ratio of Fe_3O_4 to TiO_2 was maintained as 2:1. The rest of the procedure was similar to the synthesis of SNTS nanoparticles. Subsequently, undoped TiO_2 nanocomposites were obtained as the mentioned procedure.

2.2. Characterization of samples

The X-ray diffraction (XRD) pattern of the prepared catalyst was obtained by a Seifert 3003 PTS X-ray diffractometer using Cu Kα radiation as the X-ray source in 2θ range of 20–80°. The average crystallite size of anatase phase was obtained according to Scherrer equation. The morphology of the photo catalysts was observed by MIRA3 TESCAN-XMU field emission scanning electron microscope (FESEM) equipped with an energy dispersive X-ray (EDX). The Transmission electron microscopy (TEM) images were conducted using a Philips CM30 at 150 KV. The diffuse reflectance UV/Vis (DRS-UV/Vis) spectra of the prepared photo catalysts were determined by Avantes Avaspec-2048-TEC spectrophotometer. The photoluminescence (PL) spectra of the samples were prepared by Cary Eclipse spectrometer. The N_2 adsorption and desorption isotherms were measured using Belsorp mini II. The specific surface area and pore size distribution was measured from the adsorption isotherms using Brunauer-Emmett-Teller (BET) and Barret-Joyner-Halender (BJH) methods, respectively. X-ray photo electron spectroscopy (XPS) measurements were conducted using a PHI 5000C ESCA System with Mg K$_\alpha$ source operating at 14.0 kV and 25 mA. GC/MS analyses were prepared by Agilent 7890B/5977A GC/MS equipped with HP-5MS capillary column (30 m × 0.25 mm i.d., 0.25 μm film thickness). Vibrating sample magnetometry (VSM) was prepared at room temperature to evaluate the magnetic properties of the samples (MDKFT). The concentrations of the solutions were analyzed by Varian Cary 300 UV/Vis spectrophotometer. Finally, total organic carbon (TOC) of the samples, before and after the degradation process was determined by Hach DR5000 spectrophotometer.

2.3. Evaluation of photo catalytic activity of the prepared samples

The reactor used in this research for the photo catalysis process consists of a purple LED projector lamp with dimensions of 40×40 cm (including 96, 1W purple LED lamps were purchased from Senyang Light company), which is located in a completely mirrored ambient so that its radiation property is maximized. The spectral power distribution of purple LED is presented in Fig. 1. As shown, this LED had irradiation wavelength in the range of 410–420 nm. The prepared sample which includes photo catalyst is placed inside a Vicor glass cell that is provided among the mirrors. The visible light source is located directly above the Vicor glass cell and at a distance equal to 40 cm from it. Also, it should be noted that the whole system is placed inside a protective part (metallic cabinet) so that no beam can access the external ambient.

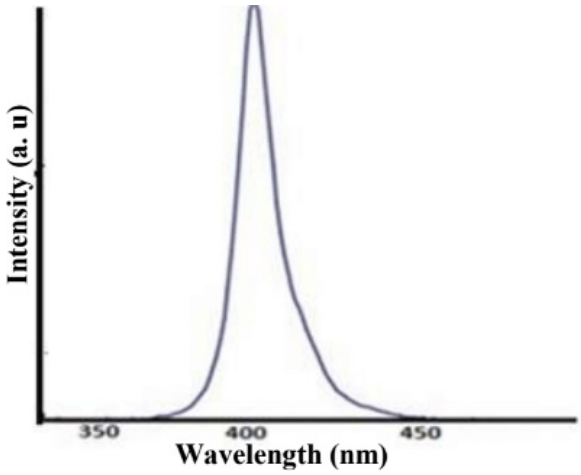

Fig. 1. Spectral power distribution of purple LED.

In order to investigate the photo catalytic activity of the synthesized nanoparticles, 100 ml of paracetamol solution has been put in contact according to the experimental design with a specific concentration in the provided Vicor glass cell. During the radiation of the visible photons, the solution was stirred continuously by a magnetic mixer. When the test begins, the photo catalysts are put in darkness for 30 min after the photo catalysts are placed in the solution (prior to turning on the LED) so as to ensure that the balance between the absorption/desorption is established on the photo catalysts surface. The values of absorption on the SNTS and SNTSF surface for PA in dark conditions were determined as 6 and 8, respectively. The produced heat from the LED is so negligible because of its low energy consumption. This property prevents heating of the environment. Therefore, fan or cooler is not required, and no fan was used.

According to the experimental design, sampling is performed at a specific time and the sample was analyzed by UV/Vis spectrometer after the separation of the nanoparticles by a centrifuge (time of 15 min and speed of 4000 rpm). In order to investigate the photo catalytic property of the nanoparticles, S and N codoped $TiO_2/SiO_2/Fe_3O_4$, these nanoparticles do not require a centrifuge for separation due to their magnetic property and can be separated by a magnet. The photo catalytic experiments under solar irradiation were performed in clear sky during August to September at the Science and Research Branch, Islamic Azad University in Tehran (latitude and longitude: 35.79084, 51.31581). Finally, the photo degradation percentage for PA was identified by spectrophotometric method in 243 nm wavelength of maximum absorbance.

2.4. Experimental design

Response surface methodology (RSM) is a set of statistical techniques used to optimize the processes in which the intended response is affected by some variables. The number of experiments has decreased and all coefficients of the quadratic regression model and interaction of the factors

can be estimated with the help of the statistical design [43]. In the present study, the response surface methodology (RSM) based on a central composite design (CCD) has been employed to optimize the operational parameters using Design Expert Software (version 7.0.0). The effects of the independent parameters including X_1 (pH), X_2 (irradiation time), X_3 (photo catalyst mass) and X_4 (PA concentration) were measured at 5 levels. Independent variables and their levels are listed in Table 1. Furthermore, the 30 experimental runs for four parameters and responses are presented in Table 2. The general equation of the response surface is defined as follows:

$$Y = \beta_0 + \sum_{i=1}^{k} \beta_i X_i + \sum_{i=1}^{k} \sum_{j=1}^{k} \beta_{i_j} X_i X_j + \sum_{i=1}^{k} \beta_{ii} X_i^2 + e_i \quad (1)$$

where Y is the predicted response (degradation percentage); β_0 is the model constant parameters; β_i, β_{ii}, β_{ij} are the linear coefficient, quadratic coefficient and interaction effect coefficient, respectively; X_i's and X_j's are the independent parameters including pH, photo catalyst mass, PA concentration and irradiation time; e_i is the model error and K is the number of factors (independent variables) [44,45].

3. Results and discussion

3.1. X-ray diffraction (XRD) analysis

The X-ray diffraction patterns of the prepared samples are shown in Fig. 2. Between the three polymorphs of TiO_2, anatase is the most activated one in photo catalytic activity, which was proved by (1 0 1), (0 0 4), (2 0 0), (1 0 5) and (2 1 1) diffraction peaks (JCPDS File no. 21-1272) [46,47]. As shown in Fig. 2, all the synthesized samples include anatase phase of TiO_2 without its two other phases which are rutile and brookite. XRD pattern of SNTSF (Fig. 2f) is consistent with a reference pattern of magnetite (JCPDS File no. 19-0629) and TiO_2 anatase phase. The crystalline sizes of the prepared photo catalysts were calculated using Debye-Scherrer equation at the main peak of anatase TiO_2 ($2\theta = 25.2°$) [Eq. (2)]

$$D = \frac{0.89\lambda 180}{\pi\beta \mathrm{Cos}\,\theta} \quad (2)$$

Table 1
Levels of factors in CCD

Factors	Levels				
	Low (–1)	Central (0)	High (+1)	−α	+α
X_1: pH	4.25	6.50	8.75	2.00	11.00
X_2: irradiation time (min)	97.5	185.0	272.5	10.0	360.0
X_3: photo catalyst mass (g)	0.057	0.105	0.152	0.010	0.200
X_4: concentration of PA (mg L^{-1})	8.75	12.50	16.25	5.00	20.00

Table 2
CCD matrix and responses

Run	X_1	X_2	X_3	X_4	Degradation %
1	2.00	185.00	0.11	12.50	93.78
2	8.75	272.50	0.06	16.25	18.87
3	4.25	97.50	0.06	8.75	92.12
4	8.75	97.50	0.06	16.25	10.8
5	8.75	97.50	0.06	8.75	36.97
6	6.50	185.00	0.11	12.50	89.99
7	6.50	10.00	0.11	12.50	43.28
8	6.50	185.00	0.11	12.50	89.96
9	8.75	272.50	0.06	8.75	51.94
10	6.50	185.00	0.11	12.50	89.99
11	8.75	272.50	0.15	8.75	57.14
12	6.50	185.00	0.11	20.00	51.87
13	6.50	360.00	0.11	12.50	64.32
14	6.50	185.00	0.11	12.50	89.90
15	6.50	185.00	0.11	12.50	89.99
16	6.50	185.00	0.11	5.00	74.98
17	8.75	97.50	0.15	16.25	40.87
18	6.50	185.00	0.01	12.50	71.56
19	6.50	185.00	0.20	12.50	84.78
20	4.25	272.50	0.06	16.25	78.89
21	4.25	97.50	0.06	16.25	82.23
22	4.25	97.50	0.15	8.75	56.32
23	4.25	97.50	0.15	16.25	93.56
24	4.25	272.50	0.15	16.25	99.98
25	4.25	272.50	0.15	8.75	70.12
26	11.00	185.00	0.11	12.50	0.00
27	4.25	272.50	0.06	8.75	99.65
28	8.75	97.50	0.15	8.75	39.78
29	8.75	272.50	0.15	16.25	49.34
30	6.50	185.00	0.11	12.50	89.97

where D is the crystal size of the synthesized samples, λ is the X-ray wavelength, and β is the full width at half maximum (FWHM) of the diffraction peak in radian. Average crystal sizes of SNTS, SNTSF and pure TiO_2 were calculated to be 19, 18 and 25 nm, respectively. In addition, regarding the sensitivity of the studied XRD method, sulfur and nitrogen phases were not found in XRD pattern and it can be concluded that S and N ions were uniformly distributed in anatase crystallite.

3.2. UV-Vis diffuse reflectance spectra (DRS) analysis

Diffuse reflectance spectra analysis (Fig. 3) was used to calculate the energy band gap of samples. The energy band gap of each sample was obtained based on the following equation:

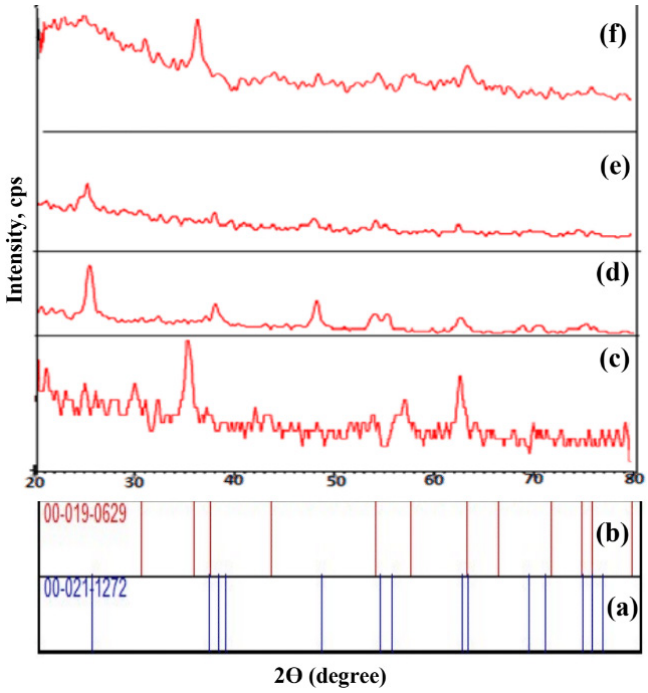

Fig. 2. XRD pattern of (a) TiO_2 anatase phase standard peaks (b) Fe_3O_4 standard peaks (c) Fe_3O_4 (d) TiO_2 (e) SNTS (f) SNTSF.

$$ahv^2 = B\left(hv - Eg\right) \quad (3)$$

where α is the absorption coefficient, *B* is a proportionality constant and ν is the frequency of photons and *Eg* is the absorption band gap [48]. The $(\alpha hv)^2$ vs. *hv* is plotted in (insert in Fig. 3) and the direct band gap of the prepared samples was obtained from the intercept of the straight line at α = 0, which is found to be 3.17, 2.86 and 2.83 eV for TiO_2/SiO_2, SNTS and SNTSF, respectively. As shown from the results, doping can improve the photo catalytic activity of TiO_2 in the visible light range. Since the energy band gap was obtained as 2.86 and 2.83 eV for SNTS and SNTSF, respectively, it is indicated that this sample can be active in purple light.

3.3. Photoluminescence (PL) analysis

Photoluminescence includes light emission caused by the made electron-hole pair recombination by light radiation [49]. For an analysis of the band-band PL process, the photoluminescence behavior of the synthesized nanocomposites was examined at an excitation wavelength of 300 nm. As shown in Fig. 4, PL intensity of prepared SNTS and SNTSF nanoparticles is lower than undoped TiO_2/SiO_2, which suggests a longer lifetime of photo generated electrons.

3.4. Field emission scanning electron microscopy (FESEM) and EDX analysis

FESEM images of TiO_2, SNTS and SNTSF are given in Fig. 5. As shown in Fig. 5b and 5c, the prepared SNTS and SNTSF catalysts are uniform and globular with less agglomeration compared to undoped TiO_2. In addition, SNTS and SNTSF nanoparticles have a lower size than undoped TiO_2. EDX analysis of prepared samples in Fig. 6 proves the presence of Ti, O, Si, S, N and Fe clearly. Furthermore, EDX Mapping of SNTSF to obtain the element distribution are given in Fig. 7.

3.5. Transmission electron microscopy (TEM)

Fig. 8 illustrates TEM images of SNTS and SNTSF nanoparticles. A core-shell structure with a core of Fe_3O_4 (black) and TiO_2/SiO_2 shell (bright) can be seen. The results are in good agreement with FESEM results and showed high globularity and the absence of any agglomeration of the prepared nanoparticles.

3.6. N_2 Adsorption/desorption analysis

Nitrogen physical adsorption method was used to investigate the surface area and porosity distribution of as-synthesized nanocomposites. BJH pore size distribution curve of SNTS and SNTSF from the adsorption branch is shown in the inset of Fig. 9 and clearly shows the mesoporous structure. The average pore size and BET results of the prepared nanocomposites with and without the presence of SiO_2 are tabulated in Table 3. The findings revealed that SiO_2 had a significant impact on enhancing the interaction between the prepared substrate and contaminants.

3.7. Vibrating sample magnetometry (VSM)

Fig. 10 shows the VSM analysis of Fe_3O_4 and SNTSF. Considering this figure, the amounts saturation magnetization (Ms) for Fe_3O_4 and SNTSF are 45.50 and 30.23 emu/g respectively. Also, the coercive force for both nanoparticles equals 0 Oe. Thus, both samples have super magnetic properties. The reduction of Ms in SNTSF is due to the non-magnetic TiO_2/SiO_2 layer and heating process during the calcination process.

3.8. X-ray photo electron spectroscopy (XPS) analysis

The surface chemical state of as-synthesized samples was additionally examined by XPS measurements. Fig. 11 depicts the XPS survey spectrum of sample SNTSF. The N 1s XPS spectra of SNTSF samples are shown in Fig. 12 (a). The N 1s peak matches three peaks placed at 398.0, 400.0, and 401.5 eV, respectively. The above peaks arise from nitrogen atom diffusion in the course of the thermal treatment, indicating a variety of N states. The present research proposes that co-doped TiO_2 exists both in the substitutional nitrogen and interstitial nitrogen fitting to the XPS data achieved in this examine. The N 1s peak is present at a binding energy of 398.0 eV lies into Ti-N bond in anatase TiO_2 lattice, suggesting the occurrence of oxygen atom substitution by nitrogen [50]. The 400.0 eV peak is attributable to the anionic N in Ti-O-N, which is the interstitial N, showing that N atoms resided into the lattice for the formation of interstitial Ti-O-N bonds [51]. The 401.5 eV peak is related to the chemisorbed N species [52].

Fig. 12 (b) depicts the high-resolution S 2p XPS spectra of SNTSF samples. There are two peaks at around

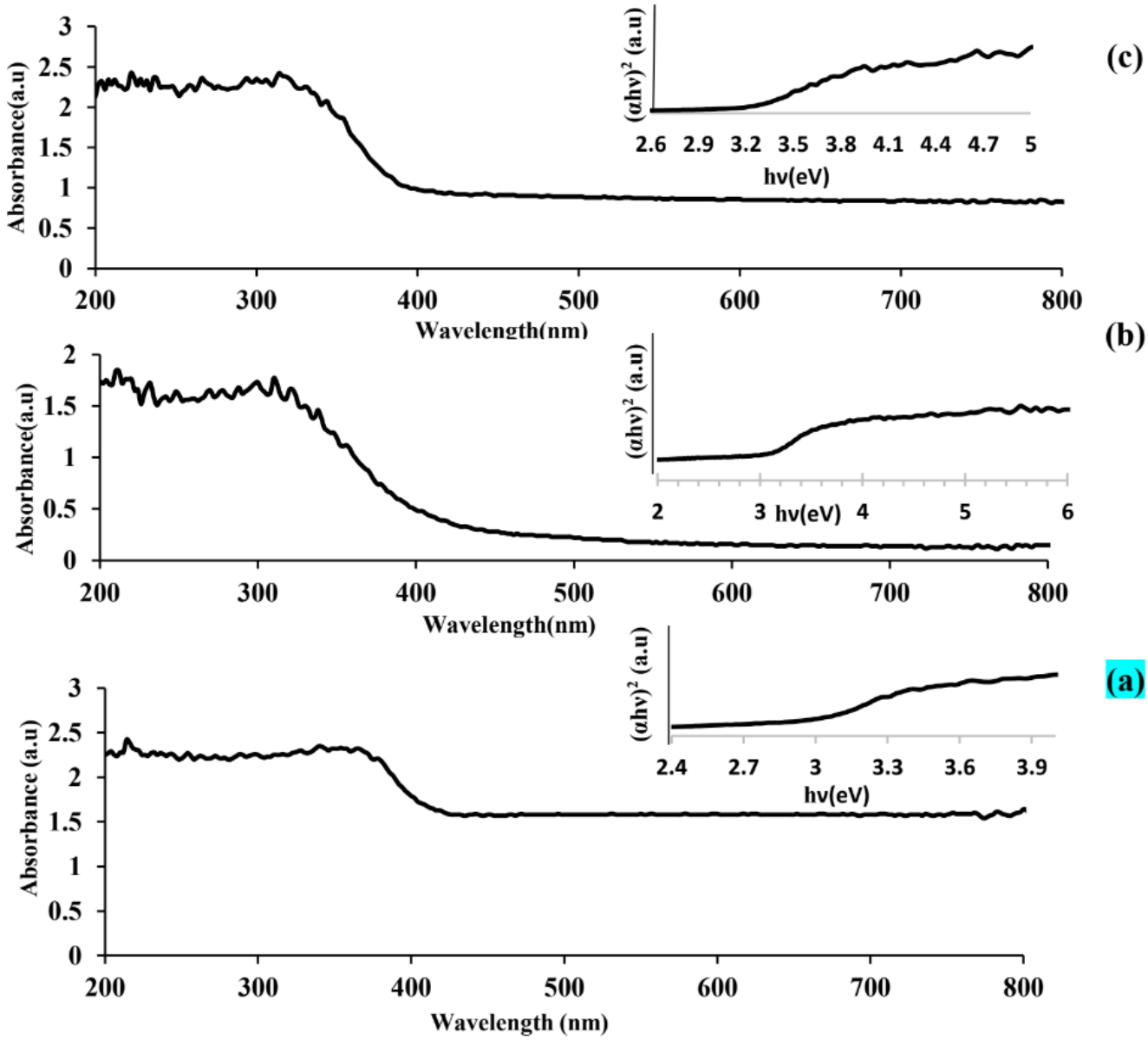

Fig. 3. DRS of SNTS (a), SNTSF(b) and TiO_2/SiO_2 (C) (the plot of $(\alpha hv)^2$ vs. hv for calculating the band gap of samples insert in their figure)

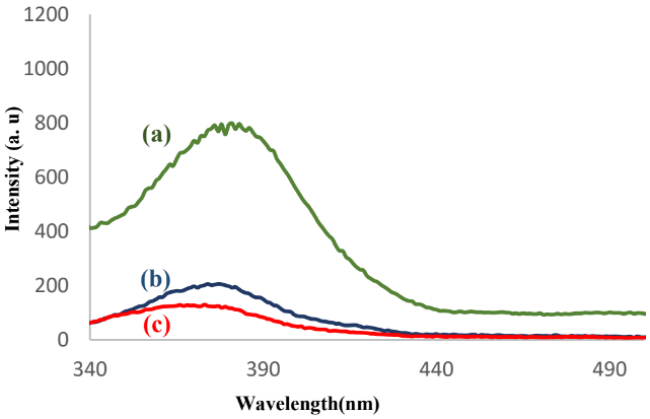

Fig. 4. PL spectra of undoped TiO_2/SiO_2 (a), SNTS (b), SNTSF (c).

168.5 and 170.0 eV, which are attributable to S^{6+} in the lattice substitute for Ti^{4+}, implying that the S specie was doped in the TiO_2 lattice [32]. It is noteworthy that there were not any peaks about 160–163 eV, corresponding to the Ti-S bond in the case of oxygen atom replacement by sulfur in the TiO_2 lattice. In chemical point of view, therefore, the replacement of Ti^{4+} by S^{6+} is more advantageous than substituting O^{2-} with S^{2-}, followed by forming Ti-O-S bonds. Earlier studies demonstrated the substitution of Ti^{4+} in TiO_2 by S^{6+} as well [32,51].

3.9. Analysis of variance (ANOVA)

Table 4 shows the analysis of variance (ANOVA) of regression factors of the response surface quadratic model

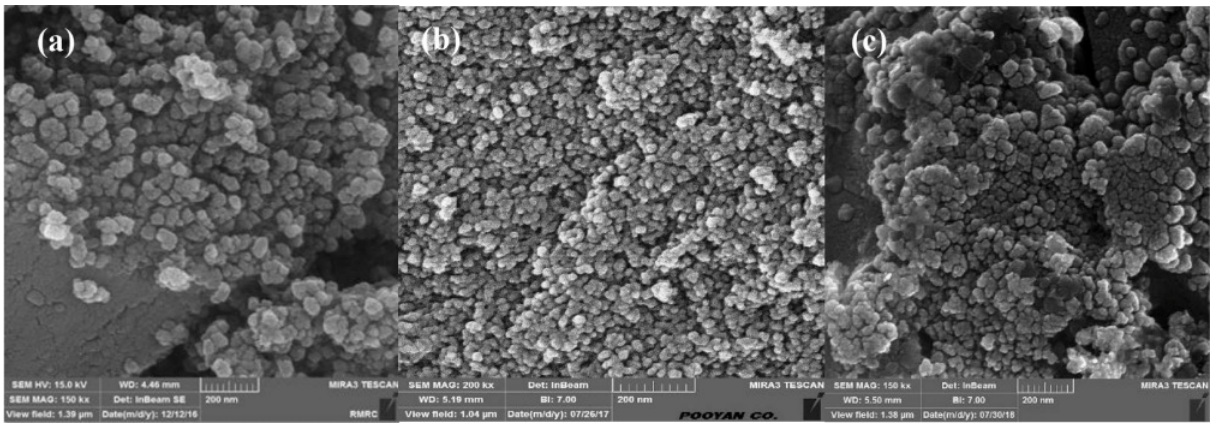

Fig. 5. FESEM images of undoped TiO_2 (a) SNTS (b) SNTSF (c).

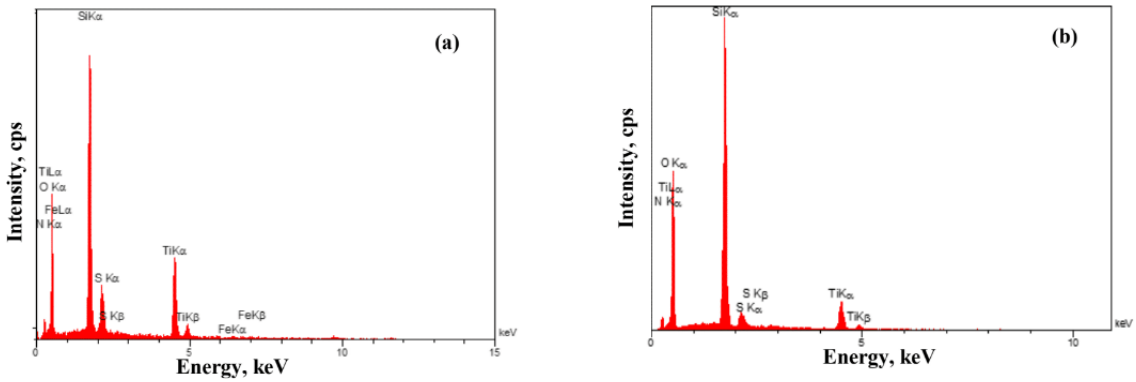

Fig. 6. EDX pattern of SNTSF (a) SNTS (b).

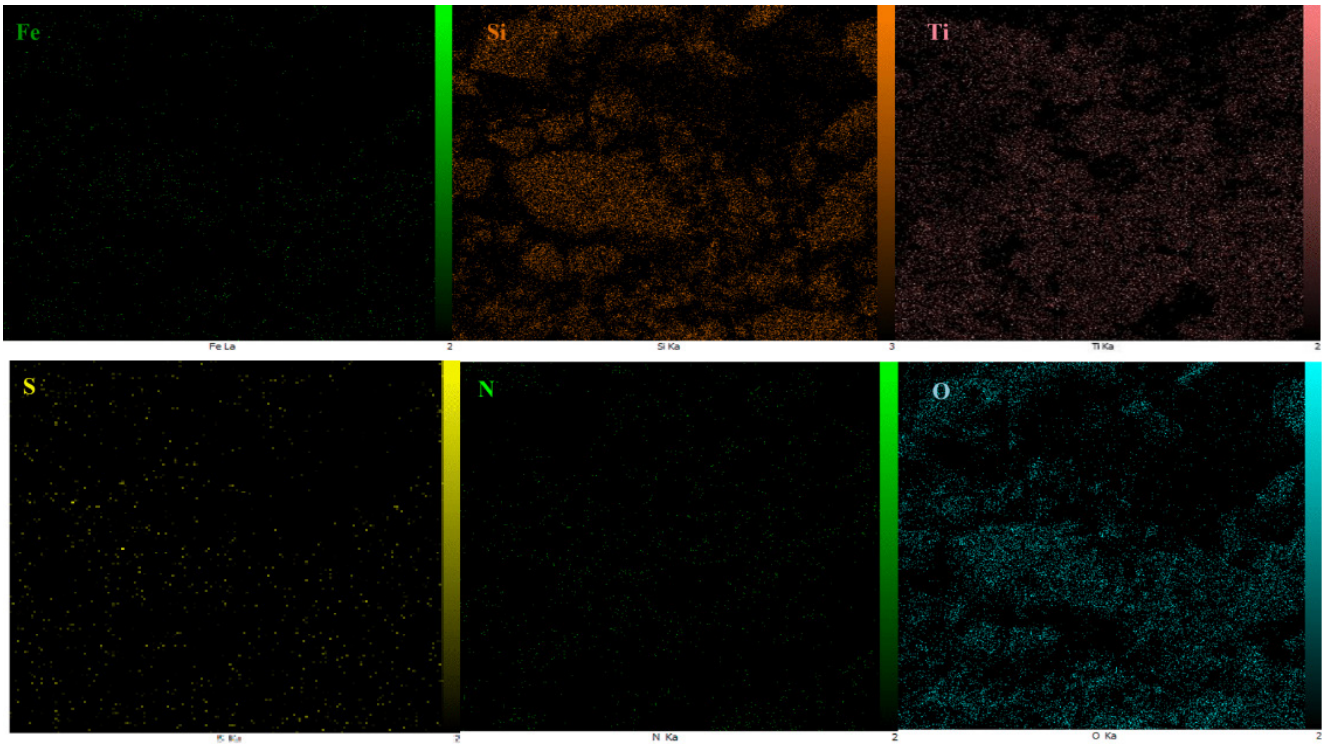

Fig. 7. EDX mapping of SNTSF.

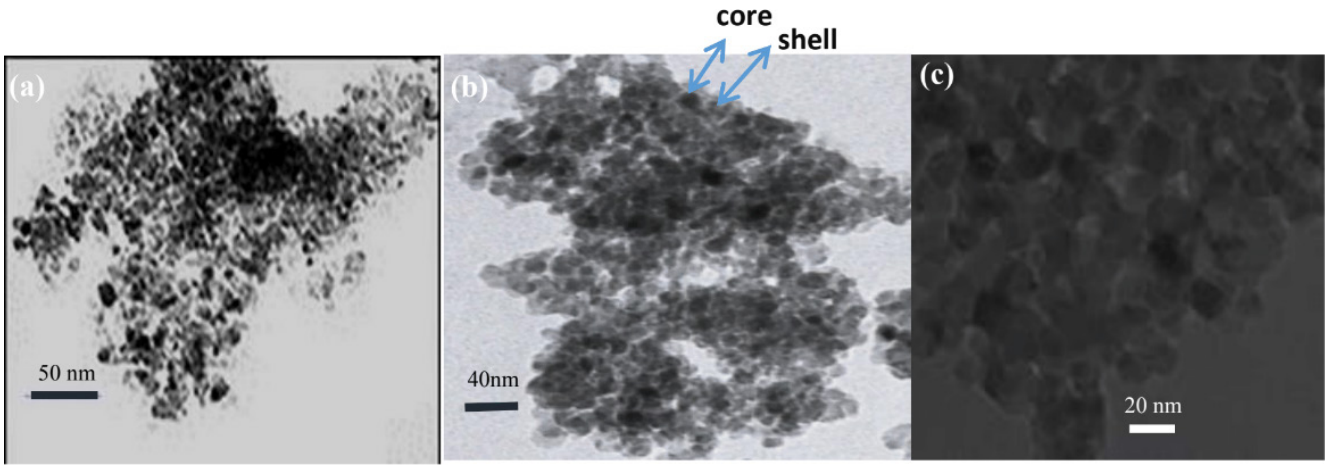

Fig. 8. TEM images of SNTSF (a, b) SNTS (c).

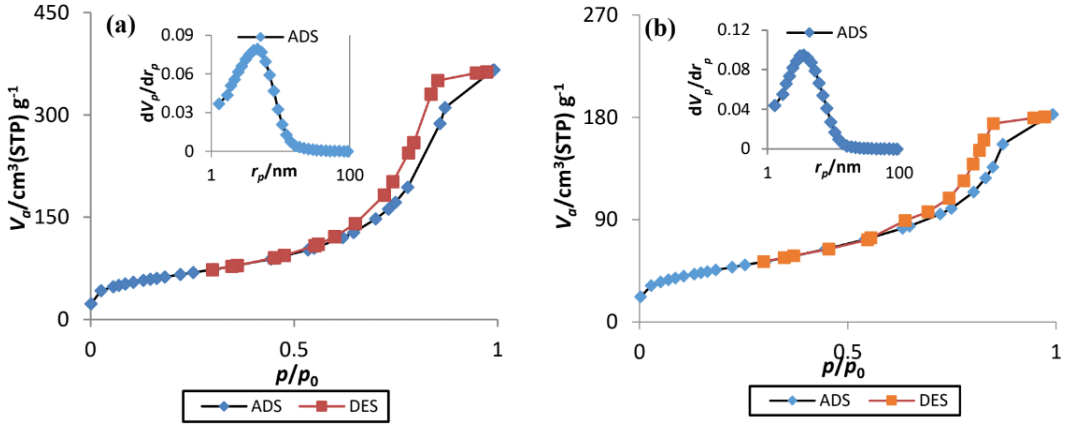

Fig. 9. N_2 adsorption/desorption isotherm of SNTS (a), SNTSF (b) (Inset: BJH pore size distribution curve).

Table 3
Physical properties of prepared samples

Samples	BET surface area (SBET) ($m^2\ g^{-1}$)	Average pore diameter (nm)
TiO_2	19.91	7.37
S-N-TiO_2	56.78	9.98
SNTS	227.50	8.13
SNTSF	195.71	8.86

for the degradation of paracetamol by SNTS. The analysis of statistical parameters and the acceptable value of the correlation coefficient (R^2 = 0.9893) demonstrates the validity of the model employed for the elimination of paracetamol. Adj-R^2 is 0.9793, which implies the high significance of the model. The P-value of less than 0.05 for a parameter shows that the parameter has a significant effect on the response [53]. As can be seen in Table 4, the P-value is less than 0.05 in the present study, which shows the validity of the model. Adequate precision implies a response to residual and the greater it becomes, the more it is preferred. The adequate precision should have a value greater than four in order for a model to show the appropriate distinction. The value of the adequate precision is 36.673 in this research. According to the analysis of variance (ANOVA), the quadratic equation based on the significant parameters for the paracetamol degradation is as follows:

Degradation of paracetamol = +89.97 – 23.11 A + 4.81 B + 2.59 C – 3.16 D + 1.53AB + 6.34 AC – 6.40 AD + 1.18 BC – 2.13 BD + 9.39 CD – 10.67 A^2 – 8.94 B^2 – 2.85 C^2 – 6.54 D^2 (4)

where *A* is pH, B is irradiation time, *C* is catalyst mass and *D* is PA concentration. Fig. 13 illustrates the perturbation diagram for paracetamol. The sharp curve of the pH (parameter A) indicates the highest efficacy of this parameter on the destruction efficiency of paracetamol. Based on the obtained results, it can be concluded that the pH and the catalyst mass are the most and least effective factors, respectively. Fig. 14 shows the normal probability plot. It is evident that the data are almost normal and the results indicate how the residuals follow a normal distribution.

3.10. Stability and re-usability of the catalysts

The stability and re-usability of the prepared catalysts were tested and great re-usability as no loss of efficiency was demonstrated inside four repetitive examinations by

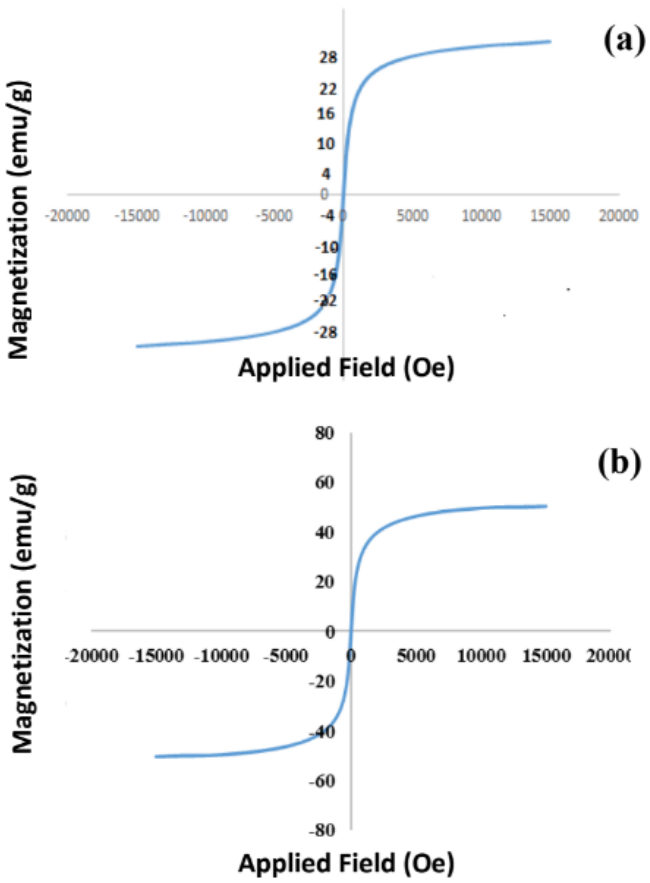

Fig. 10. Magnetic hysteresis curves of SNTSF (a) Fe_3O_4 (b) nanoparticles.

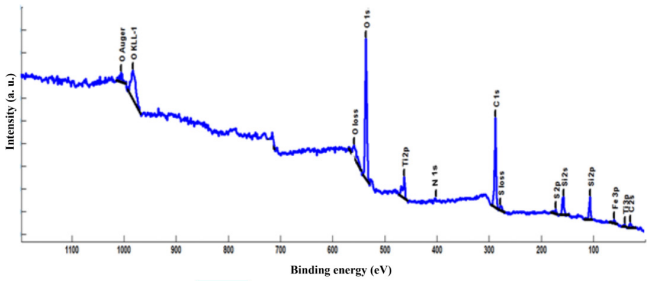

Fig. 11. XPS spectra of SNTSF.

reusing the catalysts for the degradation of PA under the optimum conditions (Fig. 15).

3.11. 3D response surface graphs

Three-dimensional surface plots are the best way to examine and visualize the effects of independent parameters on the pollutant's rate of degradation. Fig. 16a illustrates the effects of photo catalyst mass and pH on the rate of degradation of PA by SNTS in three dimensions. In this figure, the irradiation time and PA concentration are fixed and equal to 185 min and 12.5 mg L^{-1}, respectively. As evident in the figure, increasing the photo-catalyst mass and decreasing the pH lead to an increase in the destruction efficiency. The reason why the rate of destruction increases with the increase of the photo catalyst mass might be an increase in active surface sites. However, when all paracetamol molecules on the photo catalyst surface are already absorbed, a further increase in the photo catalyst (over 0.2 g) does not have much effect on the destruction efficiency. Also, high amounts of nanophotocatalyst (over 0.2 g) increase the suspension opacity; which leads to the reduction of the destruction efficiency. The pH at the point of zero charge (pH_{pzc}) for SNTS and SNTSF is 6.3 and 6.1, respectively. Due to the point of zero charge for TiO_2 at the pH about 6, the surface can act an amphoteric behavior at different pH conditions. According to Eqs. (5) and (6), Ti-OH, representing primary hydrated substrate, become negatively charged at above the pH of TiO_2 point of zero charge.

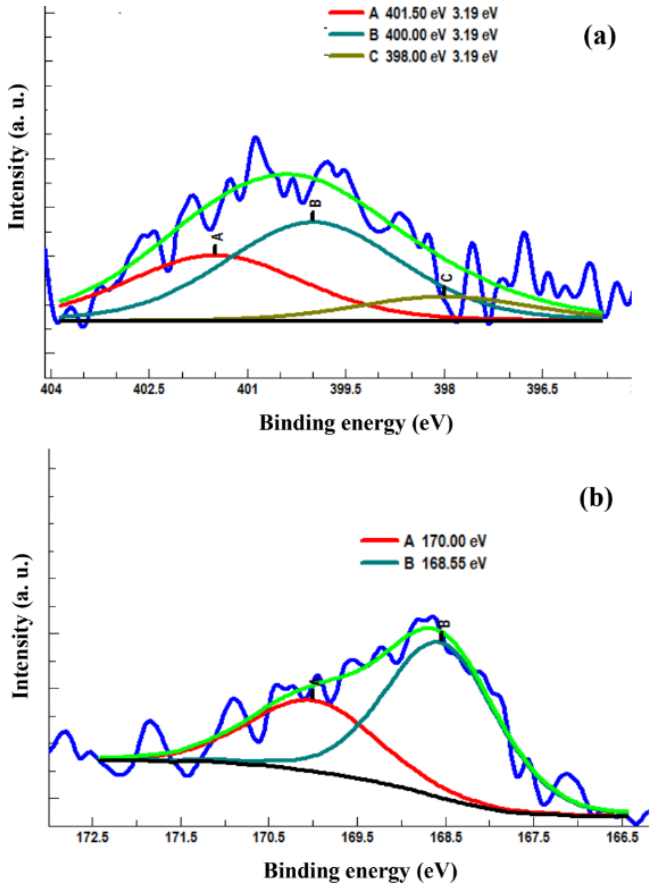

Fig. 12. High-resolution XPS spectra of the N 1s (a) S 2p (b).

$$T_i\text{-}OH + H^+ \rightleftharpoons Ti\text{-}OH_2^+ \quad (5)$$

$$T_i\text{-}OH + HO^- \rightleftharpoons Ti\text{-}O^- + H_2O \quad (6)$$

It means that at greater pH values than 6, the anionic surface of the catalyst would prevent the contaminant to adsorb on the surface to cooperate the degradation process. This fact would imply the decrease in the degradation efficiencies of the paracetamol at alkaline pH. On the contrary, at acidic pH values, the positively charged surface would electro statically attract the target anions to participate

Table 4
Analysis of variance (ANOVA)

Source	Sum of squares	df	Mean square	F value	P-value Prob > F
Model	21756.75	14	1554.05	98.97	< 0.0001 significant
A-pH	12821.43	1	12821.43	816.56	< 0.0001
B-time	554.50	1	554.50	35.31	< 0.0001
C-mass of catalyst	160.58	1	160.58	10.23	0.0060
D-concentration	238.90	1	238.90	15.21	0.0014
AB	37.39	1	37.39	2.38	0.1436
AC	643.38	1	643.38	40.98	< 0.0001
AD	655.36	1	655.36	41.74	< 0.0001
BC	22.14	1	22.14	1.41	0.2535
BD	72.42	1	72.42	4.61	0.0485
CD	1411.50	1	1411.50	89.89	< 0.0001
A^2	3123.20	1	3123.20	198.91	< 0.0001
B^2	2193.83	1	2193.83	139.72	< 0.0001
C^2	222.92	1	222.92	14.20	0.0019
D^2	1172.12	1	1172.12	74.65	< 0.0001
Residual	235.53	15	15.70		
Lack of fit	235.52	10	23.55	19199.97	< 0.0001
Pure error	6.133E-003	5	1.227E-003		
Cor total	21992.28	29			

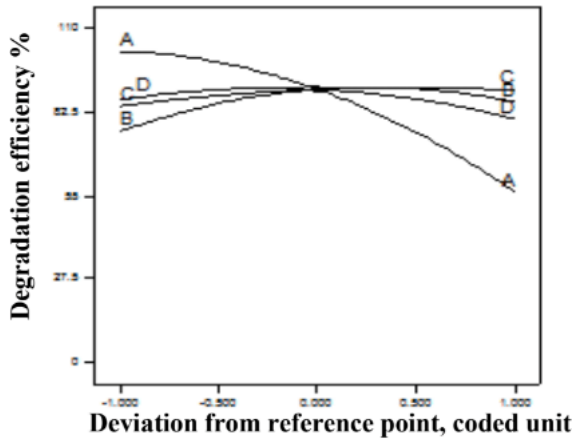

Fig. 13. Perturbation plot for degradation of PA by SNTS.

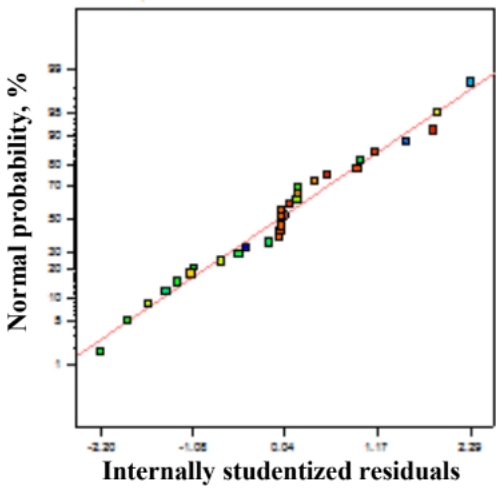

Fig. 14. Normal probability plot of the studentized residual for degradation of PA.

the degradation process that would result the increase of removal efficiencies.

Fig. 16b illustrates the effects of pH and PA concentration in three dimensions when the photo catalyst mass and irradiation time are fixed and equal to 0.11 g and 185 min, respectively. As evident, pH and PA concentration have a negative influence on degradation percentage of PA. Reducing the pH and PA concentration both lead to an increase in the destruction efficiency.

Fig. 16c plots the effects of irradiation time and pH in the photo catalyst destruction process while the PA concentration and photo catalyst mass are fixed and equal to 12.5 mg L^{-1} and 0.11 g, respectively. Increasing the irradiation time results in an increase in the rate of destruction. Based on the obtained results, the pH is the most effective factor in the destruction efficiency; followed by irradiation time, PA concentration, and photo catalyst mass.

The software reports the best point to reach the highest rate of destruction of paracetamol with a pH of 4.53, catalyst mass of 0.11 g, PA concentration of 15.24 mg L^{-1}, irradiation time of 164.53 min. As these optimum conditions, the photo

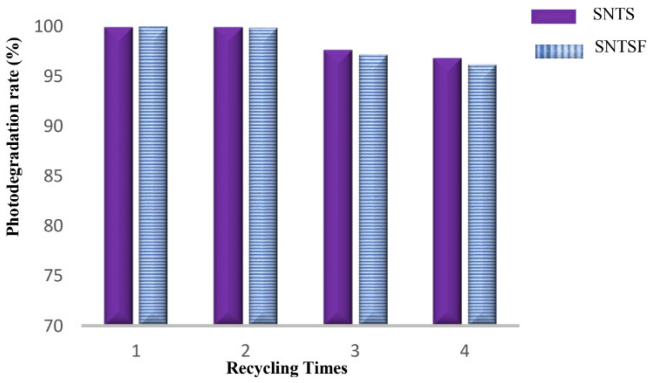

Fig. 15. Recycling tests of PA photo degradation over SNTS and SNTSF.

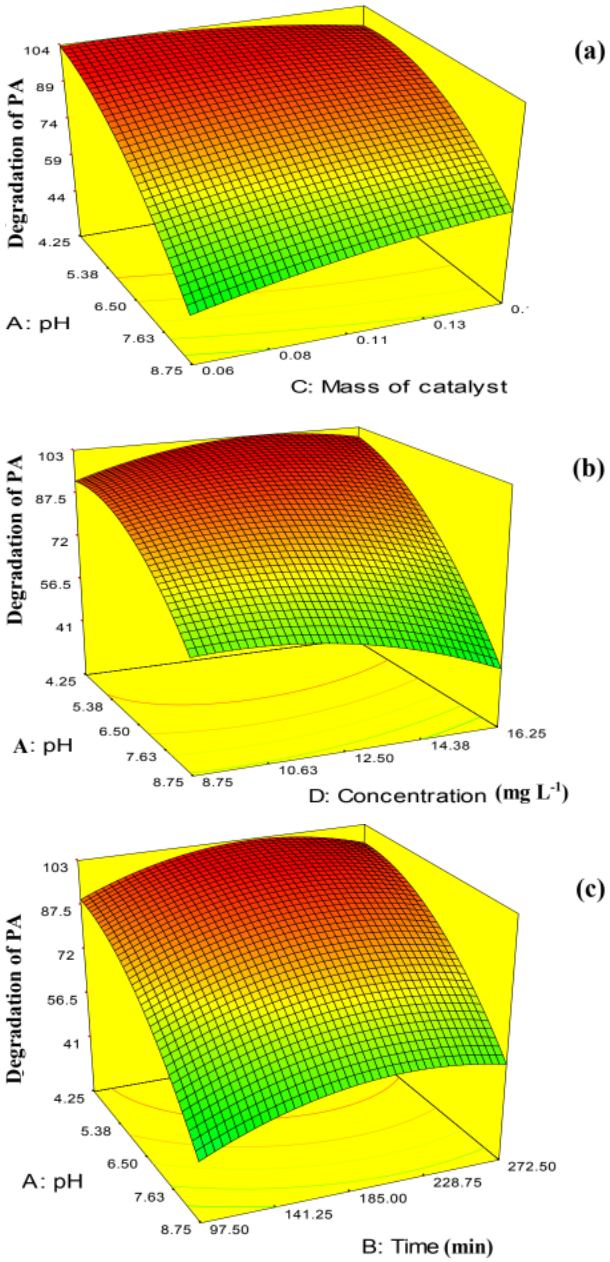

Fig. 16. 3D plots for PA degradation efficiency.

catalytic degradation percentages of PA at desirability function value of 1.0 were found to be 99.98.

3.12. Contribution of different reactive species

General descriptions about the basis and mechanism of heterogeneous photo catalysis under various light sources have been discussed previously [54,55]. The mechanism of photo catalytic degradation of PA is illustrated schematically in Fig. 17. By doping nitrogen and sulfur into the TiO_2 lattice, mid-gap energy levels such as N 2p and S 2p are formed between the O 2p valence band and the Ti 3d conduction band [56,57]. This ultimately reduces the band gap of TiO_2 and the catalyst becomes visible active. The electrons in the N 2p valence band (e^-) undergo either direct rise to the conduction band or to the S 2p and subsequently to the conduction band. H_2O molecules and/or OH^- ions are oxidized by the positive holes ($h+$) at the external surface of co-doped TiO_2, while O_2 is reduced by the excited electrons (e^-) to generate ROS ($HO^{\bullet}$ and $O_2^{\bullet-}$), with possible involvement in the photo catalytic degradation of PA.

Generally, photo catalytic reactions are conducted with the active participation of reactive oxidative species (ROS) viz; hydroxyl radical ($HO^{\bullet}$), super oxide radical anion $O_2^{\bullet-}$, hole (h^+) and electrons (e^-). The amount of participation of these ROS in the photo catalytic reaction is examined through various scavenger agents. Fig. 18 illustrates the

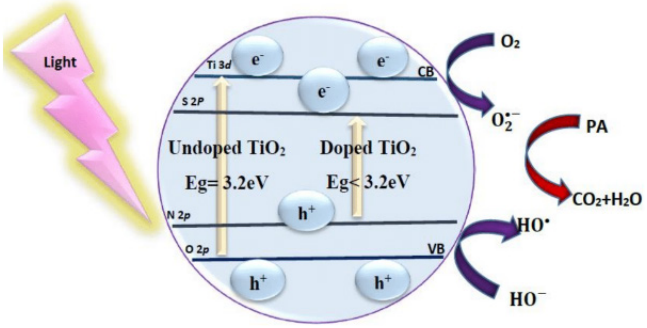

Fig. 17. Simplified photo catalytic degradation mechanism of PA using codoped TiO_2.

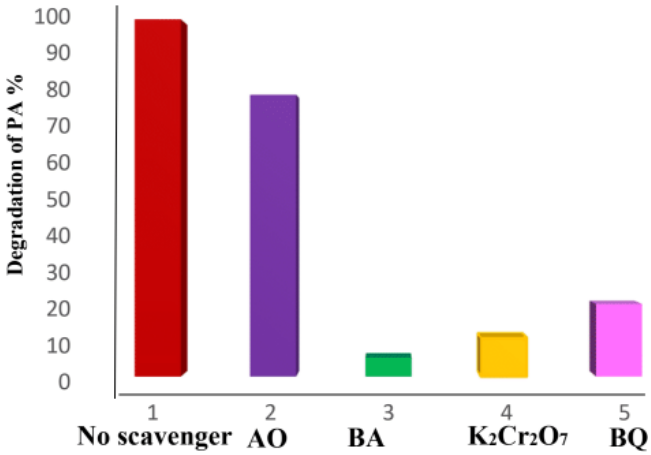

Fig. 18. Degradation efficiency of paracetamol by SNTS in the presence and absence of different scavengers.

photo catalytic activity of SNTS in paracetamol destruction in the presence and absence of various scavenger agents under the optimum conditions. In order to study the role of h^+ in the photo catalytic reaction, ammonium oxalate (AO), which is a proper h^+ scavenger [58] is added to the solution during the photo catalytic destruction process; which results in a small reduction in the rate of destruction. Furthermore, we also studied the influence of benzoic acid (BA) ($HO^\bullet$ scavenger) [59], p-benzoquinone (BQ) ($O_2^{\bullet-}$ scavenger) [60] and $K_2Cr_2O_7$ (e^- scavenger) [61]. The rate of degradation dramatically decreases by adding BA, BQ and $K_2Cr_2O_7$ scavengers. According to the results, it can be concluded that the photo catalytic destruction of paracetamol is mainly accomplished through the participation of HO it can be concluded that the photo catalytic destruction of paracetamol is mainly accomplished through the participation of $HO^\bullet$, e^- and $O_2^{\bullet-}$, respectively. Subsequently, h^+ would have less contribution to paracetamol destruction by SNTS.

3.13. Photo catalytic activity of the synthesized samples under the solar light

After achieving the optimum conditions required for the degradation of PA by SNTS, the SNTSF nanoparticles were used for degradation of the PA. SNTSF could be separated easily from the solution due to their magnetic properties. The photo catalytic effect of the SNTSF on paracetamol degradation was also studied under the same optimum conditions under sunlight and purple LED light. As previously mentioned, the photo catalytic experiments under solar irradiation were performed in clear sky during August to September at the Science and Research Branch, Islamic Azad University in Tehran. To realize the average solar insolation of Tehran during the outdoor experiments, the monthly solar insolation intensity diagram was shown in Fig. 19 [62]. The results in Table 5 revealed that SNTSF nanoparticles are able to remove paracetamol from aqueous solution as effective as SNTS nanoparticles under both purple LED and solar lights. The photo catalytic degradation products of PA on as-synthesized photo catalyst were distinguished by GC/MS technique. The results showed that 4-acetamidocatechol, 4-acetamidoresorcinol, hydroquinone, acetamide and aliphatic acids (maleic and oxalic acids) were the main products formed during the destruction of paracetamol. GC-MS chromatograms of photo catalytic degradation products of paracetamol, is shown in Fig. 20. Furthermore, to make certain the removal of organic pollutants of the wastewater, TOC analysis was performed on the samples, before and after the photo catalytic method. The results showed the percentage removal of organic content of the sample under purple LED and solar lights at 75.56 and 69.87%, respectively.

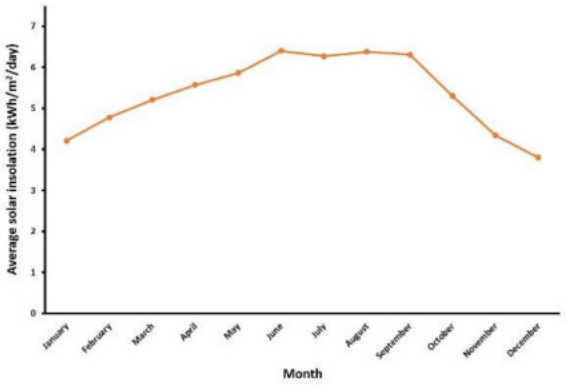

Fig. 19. Monthly average solar insolation in Tehran.

Table 5
Removal percentages acquired through various irradiation

Photo catalyst LED	Purple irradiation % Re	Solar irradiaton % Re	Without irradiation % Re
SNTS	99.98	91.85	6
SNTSF	94.82	90.23	8

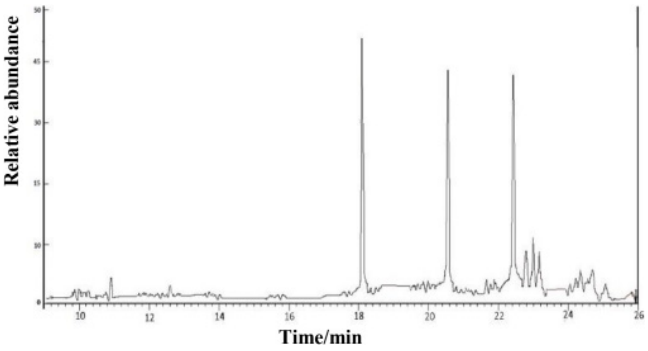

Fig. 20. GC-MS chromatograms of paracetamol degradation.

4. Conclusion

A new TiO_2/SiO_2 and magnetic $TiO_2/SiO_2/Fe_3O_4$ nanocomposites codoped with sulfur and nitrogen was successfully prepared using a sol-gel method. The photo catalytic effect of the prepared samples was investigated by removing paracetamol from the aqueous solution. The central composite design was employed to optimize the operational parameters and achievement of maximum efficiency. The optimum values for maximum efficiency using SNTS were determined at pH of 4.53, catalyst mass of 0.11 g, PA concentration of 15.24 mg L^{-1}, and irradiation time of 164.53 min. At these optimum conditions, the maximum photo catalytic degradation percentages of PA obtained was 99.98%.

Based on the results, the pH is the most effective factor in the degradation efficiency; followed by irradiation time, PA concentration, and photo catalyst mass. In addition, pH and PA concentration have a negative influence and irradiation time and photo catalyst mass have a positive influence on degradation percentage of PA. The SNTSF photo catalyst was almost as effective as SNTS. The amount of participation of reactive oxidative species in the photo catalytic reaction is investigated through various scavenger agents. Based on the results, it can be concluded that the photo catalytic degradation of PA is accomplished through the participation of , e^-, and h^+, respectively. Furthermore, great re-usability as no loss

of efficiency was proved inside four repetitive examinations by reusing the photo catalyst. Given the promising result of this research, a new study is done on the use of SNTS and magnetite SNTSF for the degradation of PA in aqueous solution by purple LED and solar irradiation.

References

[1] N. Stamatis, M. Antonopoulou, I. Konstantinou, Photo catalytic degradation kinetics and mechanisms of fungicide tebuconazole in aqueous TiO_2 suspensions, Catal. Today, 252 (2015) 93–99.

[2] K.P. Mishra, P.R. Gogate, Intensification of sonophoto catalytic degradation of p-nitrophenol at pilot scale capacity, Ultrason. Sonochem., 18 (2011) 739–744.

[3] M. Carballa, F. Omil, J.M. Lema, M.a. Llompart, C. García-Jares, I. Rodríguez, M. Gomez, T. Ternes, Behavior of pharmaceuticals, cosmetics and hormones in a sewage treatment plant, Water Res., 38 (2004) 2918–2926.

[4] M. Rabiet, A. Togola, F. Brissaud, J.-L. Seidel, H. Budzinski, F. Elbaz-Poulichet, Consequences of treated water recycling as regards pharmaceuticals and drugs in surface and ground waters of a medium-sized Mediterranean catchment, Environ. Sci. Tech., 40 (2006) 5282–5288.

[5] A. Nikolaou, S. Meric, D. Fatta, Occurrence patterns of pharmaceuticals in water and wastewater environments, Anal. Bioanal. Chem., 387 (2007) 1225–1234.

[6] X.-S. Miao, F. Bishay, M. Chen, C.D. Metcalfe, Occurrence of antimicrobials in the final effluents of wastewater treatment plants in Canada, Environ. Sci. Tech., 38 (2004) 3533–3541.

[7] D.W. Kolpin, E.T. Furlong, M.T. Meyer, E.M. Thurman, S.D. Zaugg, L.B. Barber, H.T. Buxton, Pharmaceuticals, hormones, and other organic wastewater contaminants in US streams, 1999–2000: a national reconnaissance, Environ. Sci. Tech., 36 (2002) 1202–1211.

[8] M.J. Benotti, R.A. Trenholm, B.J. Vanderford, J.C. Holady, B.D. Stanford, S.A. Snyder, Pharmaceuticals and endocrine disrupting compounds in US drinking water, Environ. Sci. Tech., 43 (2008) 597–603.

[9] O. Cardoso, J.-M. Porcher, W. Sanchez, Factory-discharged pharmaceuticals could be a relevant source of aquatic environment contamination: review of evidence and need for knowledge, Chemosphere, 115 (2014) 20–30.

[10] P.E. Stackelberg, E.T. Furlong, M.T. Meyer, S.D. Zaugg, A.K. Henderson, D.B. Reissman, Persistence of pharmaceutical compounds and other organic wastewater contaminants in a conventional drinking-water-treatment plant, Sci. Total Environ., 329 (2004) 99–113.

[11] K. Ikehata, N.J. Naghashkar, M.G. El-Din, Degradation of aqueous pharmaceuticals by ozonation and advanced oxidation processes: a review, Ozone: Sci. Eng., 28 (2006) 353–414.

[12] L. Yang, L.E. Yu, M.B. Ray, Photo catalytic oxidation of paracetamol: dominant reactants, intermediates, and reaction mechanisms, Environ. Sci. Tech., 43 (2008) 460–465.

[13] M. Jamshidi, M. Ghaedi, K. Dashtian, S. Hajati, A. Bazrafshan, Ultrasound-assisted removal of Al^{3+} ions and Alizarin red S by activated carbon engrafted with Ag nanoparticles: central composite design and genetic algorithm optimization, RSC Adv., 5 (2015) 59522–59532.

[14] M. Ghaedi, S. Hajjati, Z. Mahmudi, I. Tyagi, S. Agarwal, A. Maity, V. Gupta, Modeling of competitive ultrasonic assisted removal of the dyes–Methylene blue and Safranin-O using Fe_3O_4 nanoparticles, Chem. Eng. J., 268 (2015) 28–37.

[15] F.N. Azad, M. Ghaedi, K. Dashtian, M. Montazerozohori, S. Hajati, E. Alipanahpour, Preparation and characterization of MWCNTs functionalized by N-(3-nitrobenzylidene)-N′-trimethoxysilylpropyl-ethane-1, 2-diamine for the removal of aluminum (iii) ions via complexation with eriochrome cyanine R: spectrophotometric detection and optimization, RSC Adv., 5 (2015) 61060–61069.

[16] N. Kaur, S. Kaur, V. Singh, Preparation, characterization and photo catalytic degradation kinetics of Reactive Red dye 198 using N, Fe codoped TiO_2 nanoparticles under visible light, Desal. Water Treat., 57 (2016) 9237–9246.

[17] C.-C. Wang, J.-R. Li, X.-L. Lv, Y.-Q. Zhang, G. Guo, Photo catalytic organic pollutants degradation in metal-organic frameworks, Energ. Environ. Sci., 7 (2014) 2831–2867.

[18] Y. Wu, M. Xing, B. Tian, J. Zhang, F. Chen, Preparation of nitrogen and fluorine co-doped mesoporous TiO_2 micro sphere and photo degradation of acid orange 7 under visible light, Chem. Eng. J., 162 (2010) 710–717.

[19] M. Anpo, S. Dohshi, M. Kitano, Y. Hu, M. Takeuchi, M. Matsuoka, The preparation and characterization of highly efficient titanium oxide-based photo functional materials, Annu. Rev. Mater. Res., 35 (2005) 1–27.

[20] R. Mohamed, UV-assisted photo catalytic synthesis of TiO_2-reduced graphene oxide with enhanced photo catalytic activity in decomposition of sarin in gas phase, Desal. Water Treat., 50 (2012) 147–156.

[21] R. Mohamed, I. Mkhalid, M.A. Salam, M. Barakat, Zeolite Y from rice husk ash encapsulated with Ag-TiO_2: characterization and applications for photo catalytic degradation catalysts, Desal. Water Treat., 51 (2013) 7562–7569.

[22] C. Dette, M.A. Pérez-Osorio, C.S. Kley, P. Punke, C.E. Patrick, P. Jacobson, F. Giustino, S.J. Jung, K. Kern, TiO_2 anatase with a band gap in the visible region, Nano Lett., 14 (2014) 6533–6538.

[23] M.V. Dozzi, E. Selli, Doping TiO_2 with p-block elements: Effects on photo catalytic activity, J. Photochem. Photobiol. C., 14 (2013) 13–28.

[24] S. Bangkedphol, H. Keenan, C. Davidson, A. Sakultantimetha, W. Sirisaksoontorn, A. Songsasen, Enhancement of tributyltin degradation under natural light by N-doped TiO_2 photo catalyst, J. Hazard. Mater., 184 (2010) 533–537.

[25] G. Zhang, Y.C. Zhang, M. Nadagouda, C. Han, K. O'Shea, S.M. El-Sheikh, A.A. Ismail, D.D. Dionysiou, Visible light-sensitized S, N and C co-doped polymorphic TiO_2 for photo catalytic destruction of micro cystin-LR, Appl. Catal., B. Environ., 144 (2014) 614–621.

[26] V. Gombac, L. De Rogatis, A. Gasparotto, G. Vicario, T. Montini, D. Barreca, G. Balducci, P. Fornasiero, E. Tondello, M. Graziani, TiO_2 nanopowders doped with boron and nitrogen for photo catalytic applications, Chem. Phys., 339 (2007) 111–123.

[27] X. Ding, X. Song, P. Li, Z. Ai, L. Zhang, Efficient visible light driven photo catalytic removal of NO with aerosol flow synthesized B, N-codoped TiO_2 hollow spheres, J. Hazard. Mater., 190 (2011) 604–612.

[28] R. Pol, M. Guerrero, E. García-Lecina, A. Altube, E. Rossinyol, S. Garroni, M.D. Baró, J. Pons, J. Sort, E. Pellicer, Ni-, Pt-and (Ni/Pt)-doped TiO_2 nanophotocatalysts: A smart approach for sustainable degradation of Rhodamine B dye, Appl. Catal., B. Environ., 181 (2016) 270–278.

[29] H. Sun, G. Zhou, S. Liu, H.M. Ang, M.O. Tadé, S. Wang, Visible light responsive titania photo catalysts codoped by nitrogen and metal (Fe, Ni, Ag, or Pt) for remediation of aqueous pollutants, Chem. Eng. J., 231 (2013) 18–25.

[30] Y. Xie, Y. Li, X. Zhao, Low-temperature preparation and visible-light-induced catalytic activity of anatase F–N-codoped TiO_2, J. Mol. Catal. A: Chem., 277 (2007) 119–126.

[31] H. Khalilian, M. Behpour, V. Atouf, S.N. Hosseini, Immobilization of S, N-codoped TiO_2 nanoparticles on glass beads for photo catalytic degradation of methyl orange by fixed bed photo reactor under visible and sunlight irradiation, Sol. Energy, 112 (2015) 239–245.

[32] N. Yao, C. Wu, L. Jia, S. Han, B. Chi, J. Pu, L. Jian, Simple synthesis and characterization of mesoporous (N, S)-codoped TiO_2 with enhanced visible-light photo catalytic activity, Ceram. Int., 38 (2012) 1671–1675.

[33] M. Nasirian, Y. Lin, C. Bustillo-Lecompte, M. Mehrvar, Enhancement of photo catalytic activity of titanium dioxide using non-metal doping methods under visible light: A review, Int. J. Environ. Sci. Tech., 15 (2018) 2009–2032.

[34] J. Yu, M. Zhou, B. Cheng, X. Zhao, Preparation, characterization and photo catalytic activity of in situ N, S-codoped TiO_2 powders, J. Mol. Catal. A: Chem., 246 (2006) 176–184.
[35] A.L. Linsebigler, G. Lu, J.T. Yates, Photo catalysis on TiO_2 surfaces: Principles, mechanisms, and selected results, Chem. Rev., 95 (1995) 735–758.
[36] W. Chang, L. Yan, B. Liu, R. Sun, Photo catalyic activity of double pore structure TiO_2/SiO_2 monoliths, Ceram. Int., 43 (2017) 5881–5886.
[37] C. Anderson, A.J. Bard, An improved photo catalyst of TiO_2/SiO_2 prepared by a sol-gel synthesis, J. Phys. Chem., 99 (1995) 9882–9885.
[38] S. Islam, R.A. Rahman, Z. Othaman, S. Riaz, M. Saeed, S. Naseem, Preparation and characterization of crack-free sol-gel based SiO_2–TiO_2 hybrid nanoparticle film, J. Sol-Gel Sci. Technol., 68 (2013) 162–168.
[39] Y. Wang , Z. Xing, Z. Li, X. Wu, G. Wang, W. Zhou, Facile synthesis of high-thermostably ordered mesoporous TiO_2/SiO_2 nanocomposites: An effective bifunctional candidate for removing arsenic contaminations., J. Colloid Interface Sci., 485 (2017) 32–38.
[40] P.M. Álvarez, J. Jaramillo, F. Lopez-Pinero, P.K. Plucinski, Preparation and characterization of magnetic TiO_2 nanoparticles and their utilization for the degradation of emerging pollutants in water, Appl. Cat. B: Env., 100 (2010) 338–345.
[41] T.A. Gad-Allah, S. Kato, S. Satokawa, T. Kojima, Treatment of synthetic dyes wastewater utilizing a magnetically separable photo catalyst ($TiO_2/SiO_2/Fe_3O_4$): Parametric and kinetic studies, Desalination, 244 (2009) 1–11.
[42] M. Behpour, V. Atouf, Study of the photo catalytic activity of nanocrystalline S, N-codoped TiO_2 thin films and powders under visible and sun light irradiation, Appl. Surf. Sci., 258 (2012) 6595–6601.
[43] E.E. Kahveci, I. Taymaz, Experimental investigation on water and heat management in a PEM fuel cell using response surface methodology, Int. J. Hydro. Energ., 39 (2014) 10655–10663.
[44] J.-K. Im, I.-H. Cho, S.-K. Kim, K.-D. Zoh, Optimization of carbamazepine removal in $O_3/UV/H_2O_2$ system using a response surface methodology with central composite design, Desalination, 285 (2012) 306–314.
[45] M. Jamshidi, M. Ghaedi, K. Dashtian, S. Hajati, New ion-imprinted polymer-functionalized mesoporous SBA-15 for selective separation and preconcentration of Cr (iii) ions: modeling and optimization, RSC Adv., 5 (2015) 105789–105799.
[46] M. Pelaez, N.T. Nolan, S.C. Pillai, M.K. Seery, P. Falaras, A.G. Kontos, P.S. Dunlop, J.W. Hamilton, J.A. Byrne, K. O'shea, A review on the visible light active titanium dioxide photo catalysts for environmental applications, Appl. Catal. B: Env., 125 (2012) 331–349.
[47] M. Hamadanian, A. Reisi-Vanani, M. Behpour, A. Esmaeily, Synthesis and characterization of Fe, S-codoped TiO_2 nanoparticles: Application in degradation of organic water pollutants, Desalination, 281 (2011) 319–324.
[48] R. Mohamed, D. McKinney, W. Sigmund, Enhanced nanocatalysts, Materials Science and Engineering: R: Reports, 73 (2012) 1–13.
[49] S. Luo, Y. Xiao, L. Yang, C. Liu, F. Su, Y. Li, Q. Cai, G. Zeng, Simultaneous detoxification of hexavalent chromium and acid orange 7 by a novel Au/TiO_2 heterojunction composite nanotube arrays, Sep. Purif. Technol., 79 (2011) 85–91.
[50] E.C. Onyiriuka, Aluminium, titanium boride, and nitride films sputter deposited from multicomponent alloy targets studied by XPS, Appl. Spectrosc., 47 (1993) 35–37.
[51] J. Lv, T. Sheng, L.L. Su, G.Q. Xu, D.M. Wang, Z.X. Zheng, Y.C. Wu, N, S co-doped-TiO_2/fly ash beads composite material and visible light photo catalytic activity, Appl. Surf. Sci., 284 (2013) 229–234.
[52] J. Bu, J. Fang, F.C. Shi, Z.Q. Jiang, W.X. Huang, Photo catalytic activity of N-doped TiO_2 photo catalysts prepared from the molecular precursor $(NH_4)_2TiO(C_2O_4)_2$, Chin. J. Chem. Phys., 23 (2010) 95–101.
[53] S. Petrović, S. Stojadinović, L. Rožić, N. Radić, B. Grbić, R. Vasilić, Process modelling and analysis of plasma electrolytic oxidation of titanium for TiO_2/WO_3 thin film photo catalysts by response surface methodology, Surf. Coat. Technol., 269 (2015) 250–257.
[54] J.-M. Herrmann, Heterogeneous photo catalysis: fundamentals and applications to the removal of various types of aqueous pollutants, Catal. Today, 53 (1999) 115–129.
[55] I.K. Konstantinou, T.A. Albanis, TiO_2-assisted photo catalytic degradation of azo dyes in aqueous solution: kinetic and mechanistic investigations: a review, Appl. Catal. B: Env., 49 (2004) 1–14.
[56] C. Burda, Y.B. Lou, X.B. Chen, A.C.S. Samia, J. Stout, J.L. Gole, Enhanced nitrogen doping in TiO_2 nanoparticles, Nano Lett., 3 (2003) 1049–1051.
[57] T. Umebayashi, T. Yamaki, S. Tanala, K. Asai, Visible light-induced degradation of methylene blue on S-doped TiO_2, Chem. Lett., 1 (2003) 330–331.
[58] P.S. Kumar, S. Karuthapandian, M. Umadevi, A. Elangovan, V. Muthuraj, Light induced synthesis of Sr/CdSe nanocomposite for the highly synergistic photo degradation of methylene blue dye solution, Mater. Focus, 5 (2016) 128–136.
[59] P.S. Kumar, S.L. Prabavathi, P. Indurani, S. Karuthapandian, V. Muthuraj, Light assisted synthesis of hierarchically structured Cu/CdS nanorods with superior photo catalytic activity, stability and photo catalytic mechanism, Sep. Purif. Technol., 172 (2017) 192–201.
[60] L. Ye, J. Liu, C. Gong, L. Tian, T. Peng, L. Zan, Two different roles of metallic Ag on Ag/AgX/BiOX (X= Cl, Br) visible light photo catalysts: surface plasmon resonance and Z-scheme bridge, Acs Catal., 2 (2012) 1677–1683.
[61] T. An, J. An, H. Yang, G. Li, H. Feng, X. Nie, Photo catalytic degradation kinetics and mechanism of anti virus drug-lamivudine in TiO_2 dispersion, J. Hazard. Mater., 197 (2011) 229–236.
[62] M. Boxwell, The solar electricity handbook-2017 Edition: A Simple, Practical Guide to Solar Energy–Designing And Installing Solar Photo voltaic Systems, Green stream Publishing, 2017.